Modelling of the lateral loading of bucket foundations in sand using hydro-mechanical interface elements

Cerfontaine, B.; Charlier, R.; Collin, F.

Published in:
Numerical methods in geotechnical engineering IX

Publication date:
2018

Document Version
Peer reviewed version

Modelling of the lateral loading of bucket foundations in sand using hydro-mechanical interface elements

B. Cerfontaine
School of Science and Engineering
University of Dundee, United Kingdom

R. Charlier & F. Collin
Urban and Environmental Engineering
University of Liege, Belgium.

Accepted manuscript version of Cerfontaine, B, Charlier, R & Collin, F 2018, Modelling of the lateral loading of bucket foundations in sand using hydro-mechanical interface elements. in AS Cardoso, JL Borges, PA Costa, AT Gomes, JC Marques & CS Vieira (eds), Numerical methods in geotechnical engineering IX. vol. 2, CRC Press/ Balkema, pp. 1519-1528, 9th European Conference on Numerical Methods in Geotechnical Engineering, NUMGE 2018, Porto, Portugal, 25/06/18.

ABSTRACT:
Behaviour of offshore foundations such as piles or bucket foundations is highly dependent on interface properties. Shear mobilisation along their boundaries is crucial, not only under tension but also lateral loading. Gap opening plays an important role to develop the suction effect under bucket foundations.
Offshore foundation behaviour is often computed in purely drained (long-term) or undrained (short-term) conditions. However, dissipation of over-/under- water pressures may dissipate fast especially in sand. Subsequently in some cases the true behaviour is not purely drained nor purely undrained, but partially drained.
We developed a hydro-mechanically coupled finite element of interface able to reproduce loss of contact, friction mobilisation (Coulomb criterion), sliding, water flow along the interface and through it. Hydro-mechanical couplings arise from the definition of an effective stress, the dependence of longitudinal flow and storage to gap opening.
A bucket foundation is modelled upon lateral loading to illustrate the capabilities of the finite elements as well as the effects of couplings on the overall caisson behaviour.

1 INTRODUCTION

The exponential development of offshore renewable energy devices, exploiting wind, waves or tides, has increased the demand of innovative geotechnical engineering solutions to replace classical but sometimes costly offshore monopiles. Indeed as projects are planned in further and deeper waters, jacket superstructure or floating devices become competitive. Suction caissons or skirted foundations represent an interesting solution for wind turbine foundations, where the moment applied at the top is transferred to ground mainly via a push/pull loading (Houlsby and Byrne 2005, Houlsby et al. 2006). The partially drained behaviour due to the generated suction effect was proven to increase the strength of these foundations against transient uplift (Achmus et al. 2013, Cerfontaine et al. 2015).
The soil-caisson interface behaviour plays a crucial role in the global response of offshore foundations in general and suction caisson in particular, as reported in (Kourkoulis, Lekkakus, Gelagoti, & Kaynia 2014, Cerfontaine, Collin, & Charlier 2015). Shear mobilisation and gap opening both strongly affect the soil structure interaction. However interface simulation in partially drained conditions requires the formulation of special finite element, encompassing hydro-mechanical couplings.

Modelling of the mechanical interface problem with finite elements is not new and has been widely studied (Wriggers 2006) since the early work of Goodman (Goodman et al. 1968). Several approach were developed based on the discretisation method, the enforcement of the contact constraint or the interface constitutive law. Basically the mechanical problem relates normal and relative displacement along the interface to normal and shear stress.
In many geotechnical problems, the interface is a preferential path for fluid flow. These hydro-mechanical couplings have been devoted less attention than the purely mechanical problem over recent years (Guiducci et al. 2002, Jha and Juanes 2014, Cerfontaine et al. 2015). The interface introduces a discontinuity in the field of fluid pressures due to the longitudinal and transversal fluid flows. It is then a non-

classical fluid boundary conditions applied on each side of the solid porous bodies, since it is not pressure imposed nor flux imposed.

In this work we investigate the role of the interface in the response of a suction caisson subjected to an imposed lateral displacement. Both purely drained and partially drained simulations are carried out to illustrate the increase of strength that could be mobilised in these conditions. P-y curves related to the rigid body motion of the caisson are also derived for more practical and simplified applications.

2 STATEMENT OF THE PROBLEM

In this section we introduce the methodology used to simulate the hydro-mechanically coupled interface behaviour by the finite element method. The discretisation procedure and different couplings are defined. The constitutive law of the soil material is also defined.

2.1 *Interface finite elements*

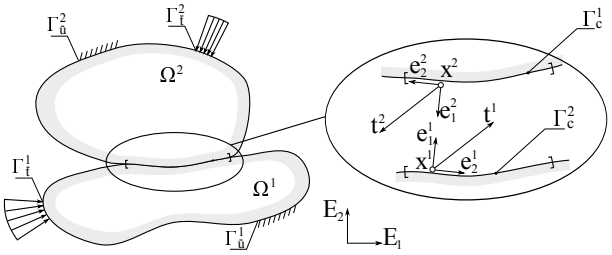

Figure 1: Definition of the contact problem between two solids Ω^1 and Ω^2.

The hydro-mechanically coupled finite element of interface is based on the zero-thickness approach (Charlier and Cescotto 1988). Boundaries of two solid porous bodies that are likely to contact are discretised using special boundary elements, having no thickness. For instance in Figure 1, the two solids Ω^i (i=1,2) are in contact along their common boundary Γ_c. If external load tends to push the solids closer, normal load increase and the surface area may increase also. If the loads tend to separate them, normal stresses release and the contact area decreases (gap creation). If a relative displacement is generated, shear stress are likely to be created. Therefore solving the mechanical contact problem requires 1) detecting the evolution of the contact zone, 2) defining a constitutive law to describe the normal/shear behaviour of the interface, 3) discretising the problem in finite elements. A detailed description of the method could be found in (Cerfontaine et al. 2015).

One of the most important variables in contact problem is the gap function g_N, which is a measure of the distance between the two sides of the interface. It is theoretically positive if there is no contact and null otherwise. There are many different ways of calculating this function (Wriggers 2006), depending on the reference system used (projection on one side or the other) or the place where it is computed (nodes, integration point). Our formulation considers that one of the two sides is given more importance (mortar/non mortar approach)(Belgacem et al. 1998). The gap function is defined at each integration point of the segments corresponding to this side with respect to the local system of coordinates (e_1, e_2, e_3).

Most of solids in contact are not able to overlap. Therefore contact between both sides generates normal stress (p_N). The ideal normal contact conditions may be summarised by the Hertz-Signorini-Moreau condition (Wriggers 2006)

$$\mathrm{g}_N \geq 0, \qquad \mathrm{p}_N \geq 0, \qquad \mathrm{g}_N \, \mathrm{p}_N = 0. \tag{1}$$

Its implementation requires a Lagrange multiplier formulation to ensure there is no interpenetration of two solids in contact. In this formulation we considered a penalty method to regularise this criterion (Charlier and Cescotto 1988). We assume that a slight interpenetration ($\mathrm{g}_N < 0$) is possible such that

$$\dot{\mathrm{p}}_N = -\mathrm{K}_N \, \dot{\mathrm{g}}_N, \tag{2}$$

where K_N is a penalty coefficient that should be appropriately defined. It should be high enough to avoid spurious a too high non-physical interpenetration of the solids but sufficiently low to avoid bad conditioning of the stiffness matrix.

Shear stresses (τ_1, τ_2) result from relative displacement between both sides of the interface. Their evolution is similarly defined with respect to variations of the relative displacement variations $\dot{\mathrm{g}}_{T1}$ and $\dot{\mathrm{g}}_{T2}$ such that

$$\dot{\tau}_{1,2} = \mathrm{K}_T \, \dot{\mathrm{g}}_{T1,2}. \tag{3}$$

The penalty coefficient related to shear stress K_T may be related to physical properties of the interface. In addition, the maximum shear stress is defined according to an elastic perfectly plastic Coulomb criterion without dilatancy such that

$$f(\mathrm{p}_N, \tau_1, \tau_2) \equiv \sqrt{\tau_1^2 + \tau_2^2} - \mu \, \mathrm{p}_N = 0. \tag{4}$$

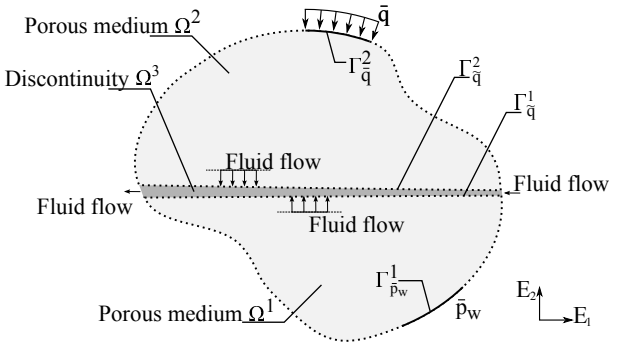

Figure 2: Definition of the flow problem corss-section of the 3D case in a plane perpendicular to the interface

The fluid flow problem within the interface is summarised in Figure 2 which is a cross-section of a 3D problem. In this case the interface models a gap between the two porous media Ω^i (i=1,2). This gap creates a new volume Ω^3 in which a fluid flow takes place. This also generates two boundary conditions $\Gamma^i_{\tilde{q}}$ (i=1,2) between Ω^3 and the porous solid bodies Ω^i. Fluid exchange takes place between inside the interface and the porous media.

The problem may be idealised as depicted in Figure 3. The field of pore water pressure is already discretised on both sides of the interface $\Gamma^i_{\tilde{q}}$. It is assumed in the following that the pore water pressure is homogeneous over the width of the gap, though it varies in both longitudinal directions. Therefore an additional field of pressure p_{w3} is discretised inside Ω^3. Additional nodes with a single degree of freedom are necessary to discretise this field.

At each integration point four fluxes must be computed as represented in Figure 3. Two of them are parallel to the interface (f_{wl1} and f_{wl2}) in both principal directions $(\mathbf{e}_2, \mathbf{e}_3)$. They are assumed to obey the Darcy's law such that,

$$\mathrm{f}_{wl(i-1)} = -\frac{k_l}{\mu_w}\left(\nabla_{\mathbf{e}_i}\mathrm{p}_{w3} + \rho_w\,\mathrm{g}\,\nabla_{\mathbf{e}_i} z\right)\rho_w \qquad \text{for} \quad i = 2,3 \tag{5}$$

where $\nabla_{\mathbf{e}_i}$ is the gradient in the direction $\mathbf{e}_i$, μ_w is the dynamic viscosity of the fluid, g the acceleration of gravity, ρ_w is the density of the fluid and k_l is the permeability.
Two other fluxes are perpendicular to the interface (f_{wl1} and f_{wl2}). They represent the exchange between the the porous media and the interface. They depend on the drop of pressure between each side of the interface and inside it such that

$$f_{wt1} = \rho_w\,\mathrm{T}_w\left(\mathrm{p}_{w1} - \mathrm{p}_{w3}\right), \tag{6}$$

$$f_{wt2} = \rho_w\,\mathrm{T}_w\left(\mathrm{p}_{w3} - \mathrm{p}_{w2}\right), \tag{7}$$

where p_w denotes a water pressure, T_w is a transversal conductivity and ρ_w is water density.

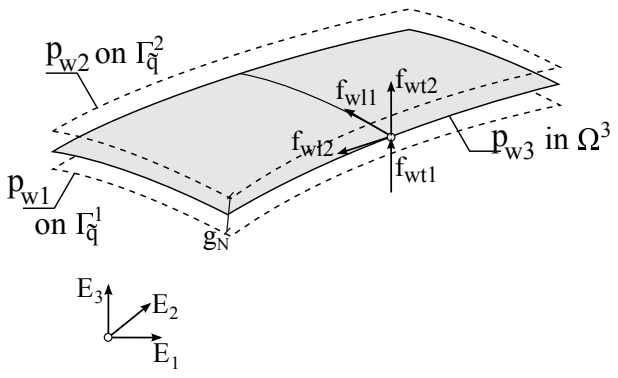

Figure 3: Definition of transversal and longitudinal fluid flows

The formulation induces three hydro-mechanical couplings. The normal pressure acting on each side of the interface is decomposed into an effective normal pressure (and a pore water pressure, according to the Terzaghi's definition

$$\mathrm{p}_N = \mathrm{p}'_N + \mathrm{p}_w. \tag{8}$$

The effective normal pressure is used in the mechanical part of the model (contact detection and Coulomb criterion).

The void created when two side saturated bodies lose contact introduces a storage term in the fluid mass balance equation. In this work the variation of the total mass of fluid $\dot{\mathrm{M}}_f$ stored in Ω^3 comes mainly from the opening/closing of the gap if the fluid is assumed incompressible, namely

$$\mathrm{d}\dot{\mathrm{M}}_f = \rho_w\,\dot{\mathrm{g}}_N\,\mathrm{d}\Gamma_{\tilde{q}}, \tag{9}$$

where $\mathrm{d}\Gamma_{\tilde{q}}$ is an infinitesimal part of the interface area.

Finally longitudinal permeability used in the Darcy's law depends on the side of the gap g_N according to a cubic law such that

$$k_l = \begin{cases} \dfrac{(\mathrm{D}_0)^2}{12} & \text{if} \quad \mathrm{g}_N \le 0 \\ \dfrac{(\mathrm{D}_0 + \mathrm{g}_N)^2}{12} & \text{otherwise.} \end{cases} \tag{10}$$

If contact exists ($\mathrm{g}_N \le 0$), the gap is negative and permeability should be equal equal to zero. However from a physical point of view, there could be a path for fluid flow through asperities of a rough surface (residual opening). Moreover from the numerical point of view, a null permeability may lead to a badly conditioned problem. Therefore a very low residual opening D_0 is added. Hence, the permeability is computed according to (Olsson & Barton 2001, Guiducci, Pellegrino, Radu, Collin, & Charlier 2002).

2.2 *Numerical model*

A steel suction caisson is assumed embedded in an homogeneous sandy soil layer as shown in Figure 4. Interface elements are set up all along the boundary between the soil and the caisson. The radius of the soil layer is equal to 24m and its depth to 12m. The mesh comprises 16058 nodes and 14190 eight-node elements. The caisson whose parameters are provided in Table 1, is composed of a rigid lid at the top and a vertical skirt. It is 7.8m diameter and its length is equal to 4m. The lateral loading consists on an imposed lateral displacement at the top centre of the caisson. The installation is not modelled and the caisson is supposed wished in place. The initial stresses within the surrounding soil are defined using a K_0 coefficient equal to 1. A confinement corresponding to 1m of soil is applied at the soil surface.

The mechanical behaviour of the caisson is assumed purely elastic. It is also deemed impervious.

Table 1: Geometrical parameters: R_{int} inner radius, R_{out} outer radius, L length, t_{skirt} thickness of the skirt, t_{lid} thickness of the lid.

R_{int}	R_{out}	L	t_{skirt}	t_{lid}
3.8m	3.9m	4m	0.1m	0.4m

The behaviour of the soil is modelled through the elastoplastic internal friction model PLASOL, implemented in the finite element code LAGAMINE (Barnichon 1998). The law is based on friction angle hardening from the initial ϕ_i to the final ϕ_f friction angle, as a function of the deviatoric plastic deformation ϵ^p_{eq} according to

$$\phi = \phi_i + (\phi_f - \phi_i)\frac{\epsilon^p_{eq}}{B_\phi + \epsilon^p_{eq}}, \tag{11}$$

where B_ϕ is a material parameter. The effective weight of the soil is equal to 10.56kN/m^3 while its permeability is equal to 1.E-4 m/s. The soil caisson friction coefficient is equal to 0.5. All material parameters are defined in Table 2.

Table 2: Material parameters: E Young modulus, ν Poisson's ratio, K_N, K_T penalty coefficients, μ friction coefficient, T_w transversal conductivity.

Soil				
E [MPa]	ν [-]	ϕ_i [°]	ϕ_f [°]	B_ϕ [-]
2E2	0.3	5	30	0.005
Caisson				
E [MPa]	ν [-]			
2E5	0.3			
Interface				
K_N/K_T [N/m^3]		μ [-]	T_w [m.Pa^{-1}.s^{-1}]	
1E10		0.50	1.E-8	

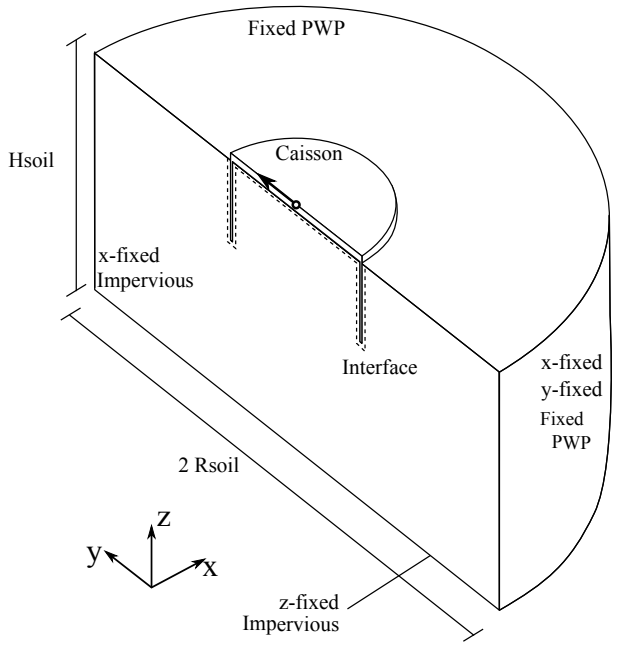

Figure 4: Global sketch of the problem geometry

3 RESULTS

In this section we analyse the lateral loading of the caisson previously defined in drained and partially drained conditions. In the first case the pore water pressure within the soil are not allowed to vary. In the second case, pore water pressure are generated and dissipated during loading, leading to partially drained conditions (not totally drained and not totally undrained). The global load displacement relation is explained in the light of the interface behaviour.

3.1 *Drained simulation*

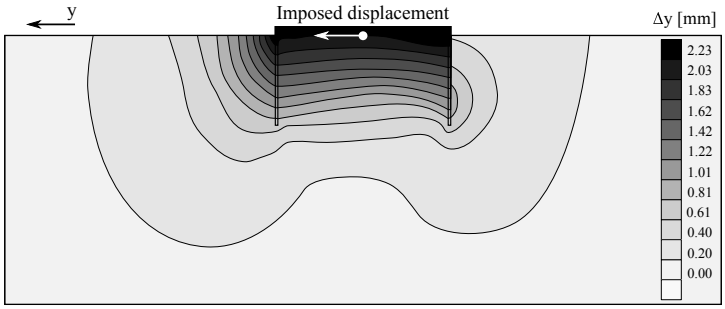

Figure 5: Cross section of the lateral displacement $\Delta y[mm]$ in the central vertical plane, drained simulation after a lateral imposed displacement of 2.5mm

The soil in front of the caisson is progressively loaded due to the imposed lateral displacement. As a consequence it starts plastifying from the surface, where the strength is the lowest, due to the low confinement. Therefore the soil lateral movement is larger close to the surface, as reported in Figure 5. A wedge of highly loaded soil is formed in front of the caisson. Subsequently it tends to rotate, as described in Figure 6.

The lateral loading induces an increase in normal stress within the front interface. Therefore maximum shear stress available is increased and the soil around is pushed down due to the rotation movement. On the contrary at the back of the caisson, there is a discontinuity between vertical/lateral displacement of the soil and caisson. This is due to the creation of a gap between them. In this zone, no shear stress can be generated. This gap may be important if the caisson must face an uplift load since it creates a preferential path to drain fluid flow from inside it.

Inside the caisson, the soil seems plugged and accompanies the caisson movement. However the slight discontinuity of vertical displacement between soil and caisson at the top may indicate a very small gap. In conclusion the caisson movement may be summarised as the combination of three rigid movements: 1) a lateral displacement, 2) a slight vertical movement and 3) a rotation with respect to the top centre.

Cross-sections of the normal effective and shear stress along the interface are useful to understand how the caisson behaves. They are represented radially in a 2D plot as sketched in Figure 7. Results are normalised and depicted with respect to the initial position of the caisson. If we consider each radial direction, we can define

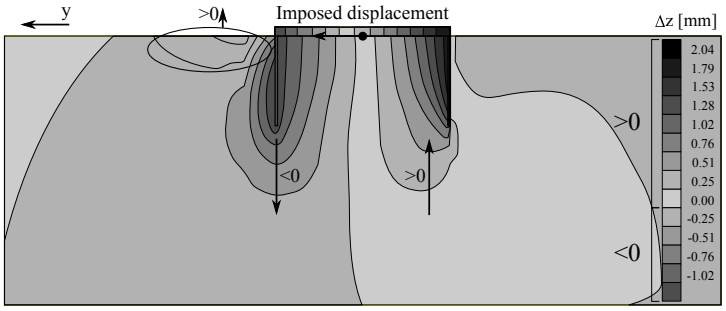

Figure 6: Cross section of the vertical displacement $\Delta z[mm]$ in the central vertical plane, drained simulation after a lateral imposed displacement of 2.5mm

- an application point: the intersection between radial direction and trace of the caisson;
- a magnitude: distance between the application point and the trace of results;
- a sense: positive (outside the trace of the caisson), negative (inside).

Cross-sections of the normal effective stress at four different depths is provided in Figure 8 after 2.5mm of imposed lateral displacement. This figure confirms the creation of a gap which is larger is size at the top than at the bottom of the caisson. It also exhibits that the main reaction component to the loading is obviously the increase in normal load. This load increases the initial stress within the soil by approximatively 50%.

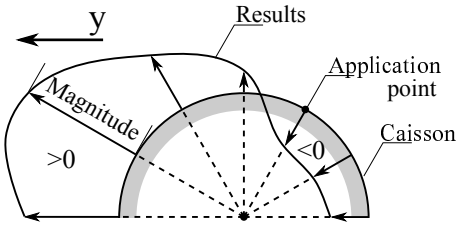

Figure 7: Normalised radial distribution of results within interface

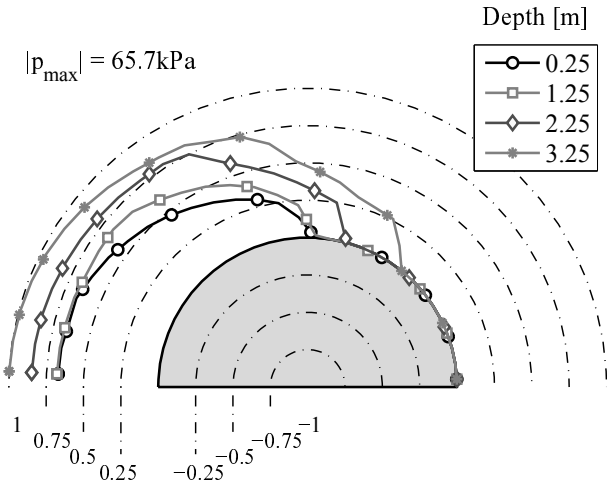

Figure 8: Distribution of normal effective in horizontal cross-sections at different depths, drained simulation

Cross-section of the projection of the shear stress in the y direction are provided in Figure 9. This underlines that friction plays a non-negligible role in the resistance to lateral loading. This value at the front is equal to zero since the tangent to the caisson is perpendicular to the loading direction. It increases progressively with the direction of the radial direction. It is obviously null at the back of the caisson since there is a gap.

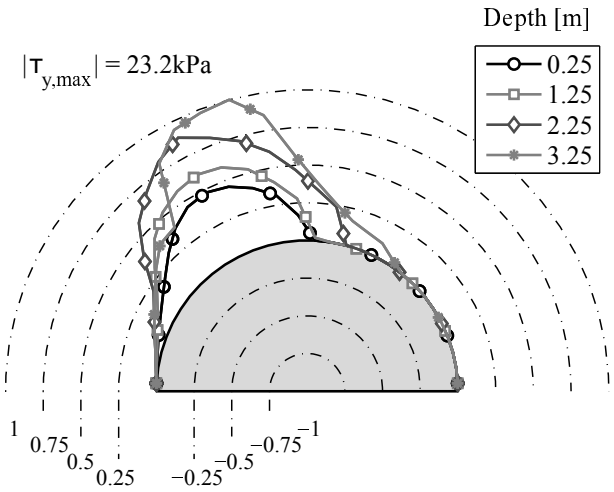

Figure 9: Distribution of shear stress projected in the y direction in horizontal cross-sections at different depths, drained simulation

The total horizontal (ΔF_{tot}) load versus lateral displacement (Δy) is represented in Figure 10. It presents a classical shape with a clear change of slope after around 2mm of imposed displacement (Achmus and Thieken 2010, Bienen et al. 2012). Before the slope breakage, initial stresses at the back of the caisson are released and stresses in front increase. This is similar to an elastic unloading. After the slope breakage, a gap is formed and there is no more unloading. The global tangent stiffness corresponds only to the loading of the soil in front of the caisson.

Rotation of the caisson generates a relative vertical displacement between the caisson and the soil, giving birth to non-zero vertical shear stresses inside and outside the caisson. The integration of the stresses over the surface is summarised into ΔF_{in} and ΔF_{out} variables, as reported in Figure 10 and sketched in Figure 11.

The shear components have different magnitudes and signs. Direction of shear forces is directed upwards at the front of the caisson and downwards behind it due to the rotation. However the magnitude of shear stress is different in absolute value between inside and outside the caisson, due to the gap opening (outside at the back). Maximum friction is reached in both cases since a plateau is attained.

In addition, shear is mobilised at the base of the caisson. It may lead to a global failure if the shear capacity is reached. However it is not in this case since the caisson has a large diameter. Finally the pore water pressure variation is null since drained conditions are

considered.

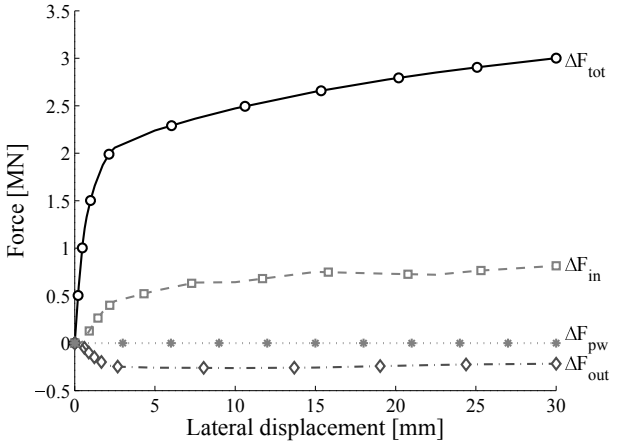

Figure 10: Variation of total horizontal load ΔF_{tot}, PWP under the lid ΔF_{pw} and shear forces $\Delta F_{in}/\Delta F_{out}$, drained simulation

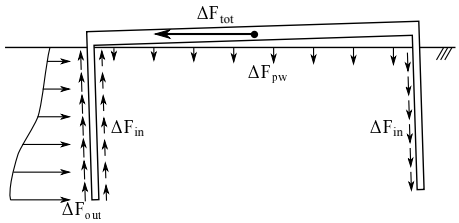

Figure 11: Definition of different components

3.2 *Partially drained simulation*

During the partially drained simulation the rate of imposed lateral displacement is 0.05 mm/s. The total horizontal load is compared with the drained result in Figure 12. During the first part of the loading, before the slope breakage, both responses are almost identical. However they diverge afterwards due to the late mobilisation of a pore water pressure effect. Subsequently the capacity of the caisson is increased if larger displacement is allowed.

Indeed suction effects within interface oppose to gap creation. This could be observed in Figure 13. Negative variations of pore water pressure are generated inside at the front close to the top due to the complex movement. It is also negative right under the lid, restraining the rotation movement. The integration of pore water pressure variations under the lid are gathered into ΔF_{pw}, presented in Figure 12. Finally negative variations are even surprisingly noted at the back outside of the caisson, close to the bottom. They also oppose gap creation, despite these underpressures are more easily dissipated. However this effect may suddenly disappear as the gap opening increases vertical permeability within the interface. Therefore if the gap opens up to the surface where water pressure is fixed, the negative overpressure is expected to suddenly disappear.

The distribution of normal effective stress p'_N in horizontal cross-sections is depicted in Figure 14. The

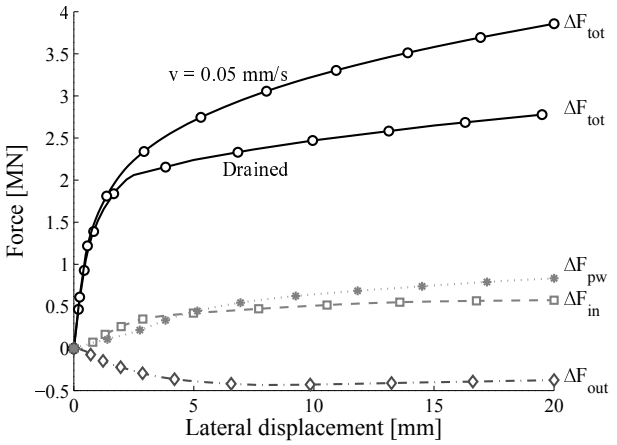

Figure 12: Variation of total horizontal load ΔF_{tot}, PWP under the lid ΔF_{pw} and shear forces $\Delta F_{in}/\Delta F_{out}$, partially drained simulation

partially drained conditions do not increase significantly the maximum normal effective stress in front of the caisson. However as previouly mentioned, it reduces the gap opening at the back (zones where $p'_N = 0$). This is evident by comparison with Figure 8.

The distribution of pore water pressure outside of the caisson follows an opposite pattern. It is almost null at the front where there is no gap and pore water pressures generated by soil volumetric reduction are fast dissipated. However it is negative at the back where gap tends to open and creates this suction effect.

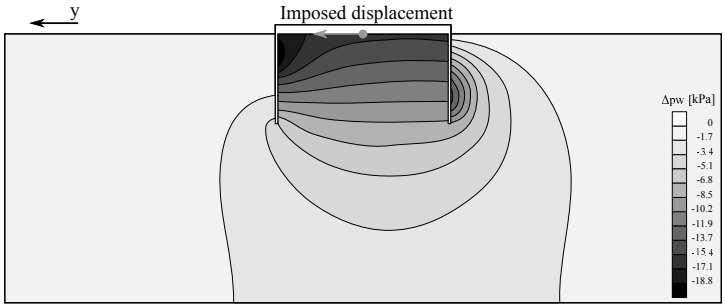

Figure 13: Cross section of pore water pressure variations Δp_w [kPa] in the central plane, drained simulation after 20mm , partially drained simulation

The drained and partially drained p-y curves are represented in Figure 33 for comparison. Each p-y curve includes different components acting on each side of the caisson: normal effective pressure, horizontal shear stress and pore water pressure. The curves close to the surface (depth = 0.25m) have more or less an identical shape. All others partially drained curves exhibit an increase in force for an identical displacement. The distribution of effective stress around the shaft is not really modified as depicted in Figure 34a. Only the gap is less open since the normal pressure is not equal to zero behind the caisson (depth = 3.25m). Therefore it could be reasonably stated that the difference between p-y curves is due to the pore pressure distribution.

P-y curves are often defined for piles (Reese and Van Impe 2010). They represent lateral load p mobilised within the soil per meter depth, opposing a

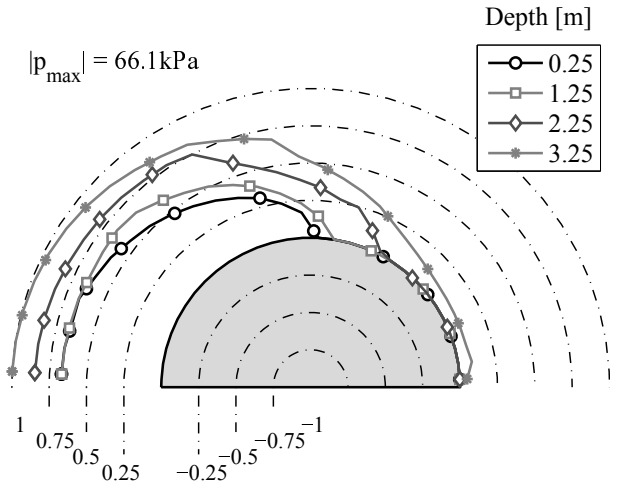

Figure 14: Distribution of normal effective in horizontal cross-sections at different depths, drained simulation after a lateral imposed displacement of 2.5mm

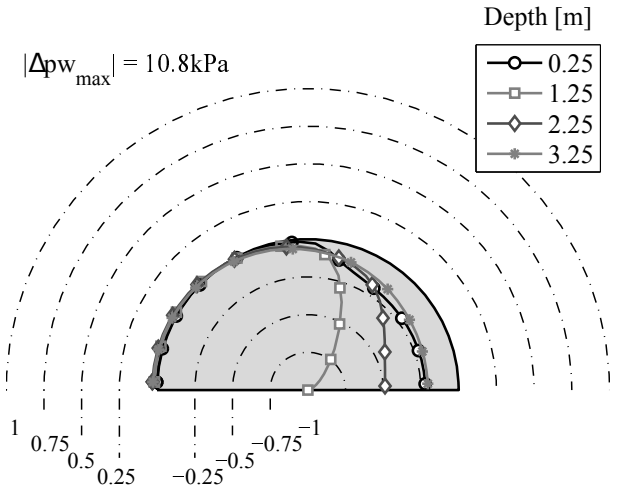

Figure 15: Distribution of pore water pressure out side of the caisson in horizontal cross-sections at different depths, drained simulation after 2.5mm

given displacement y. Similarly the normal and tangential stresses as well as pore water pressure can be integrated along the boundaries of the caisson. However the modelled caisson is far from a pile: it has a length to diameter ratio of 0.5. Firstly the caisson should be modelled like a rigid body rather than a bending pile. Secondly, the p-y curves result from the difference between inside and outside reactions from the soil onto the caisson, in the y direction. The y displacement is the displacement of the mean fibre of the caisson, at each depth.

The force versus displacement is provided at four depths in Figure 16 in drained and partially drained conditions. This figure confirms two previous observations: 1) load mobilised increases with depth, 2) the larger displacement at the top of the caisson indicates a rotation. The curve shapes are also similar to the global load displacement relation. Indeed the slope breakage corresponds to the gap opening. It appears for a larger displacement in drained conditions as depth increases. However transition becomes smoother as partially drained conditions are consid-

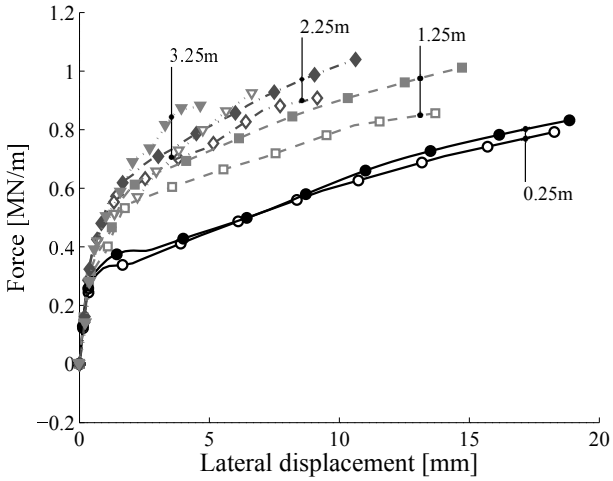

Figure 16: Comparison of p-y curves at different depths in drained (open markers) and partially drained (filled markers) conditions

ered. The effect of partial drainage is to shift the p-y curves up, mobilising a high load for a given displacement. This is mainly due to the pore water pressure effect and does not appear close to the surface where these pore pressure are fast dissipated.

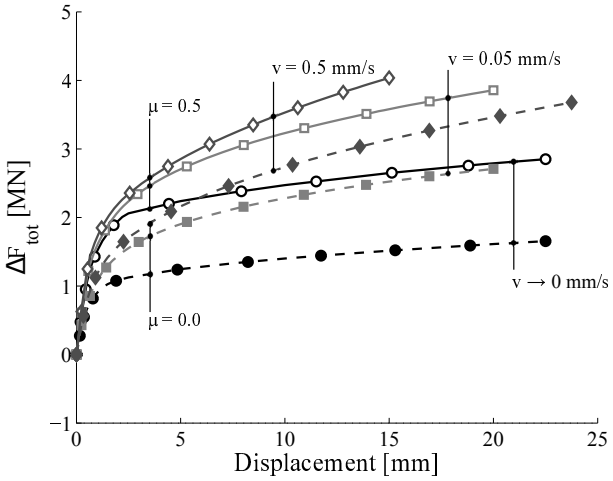

Figure 17: Variation of total horizontal load ΔF_{tot} for different horizontal loading rate (v) and friction coefficients (μ)

The influence of the loading rate and friction coefficient and depicted in Figure 17. The partially drained effect seems to decrease at higher loading rate. Indeed increasing the loading rate from 0.05mm/s to 0.5mm/s only slightly raises the total load mobilised.

It could be assumed that friction plays a minor role in the strength development towards lateral loading, contrary to normal reaction of the soil. However results prove that friction is crucial. In the drained case, The mobilised load drops to half of the value if there is no shearing allowed to develop along the shaft. This effect is still important in partially drained conditions. This drop is probably due to the lose of horizontal shearing along the shaft. In addition the rotation movement is not balanced by friction any more, resulting in a different load distribution.

4 CONCLUSIONS

Throughout this work, we have proven that interface behaviour is crucial in the modelling of lateral loading of suction caisson foundation. Opening of gap and shear mobilisation both strongly influence the strength, stiffness and shape of the load-displacement curve. The partially drained behaviour, induced by generation and dissipation of negative pore water pressures is shown to increase the total horizontal resistance for a given displacement. It also opposes to gap opening. This is particularly important since vertical gap may strongly affect the vertical behaviour by introducing preferential path to dissipate inner negative fluid pressures as reported in (Cerfontaine et al. 2015, Cerfontaine et al. 2015).

For all of these reasons the development of hydro-mechanically coupled finite elements of interface is necessary. They must take into account gap opening, shear mobilisation, longitudinal and transversal fluid flows. In this work the zero-thickness approach is coupled with a three-node formulation to discretise the field of pressure inside the interface. Hydro-mechanical couplings arise from the definition of an effective mechanical contact pressure, the dependence of the longitudinal permeability on the gap opening and the definition of a storage term in the mass balance equation as the gap opens.

P-y curves were also defined similarly to piles. They relate the mobilisation of shear along the shaft and normal pressure to the lateral displacement of the caisson. They are obtained from variables available in the interface elements. Such p-y curves could be used to model the caisson as a rigid body connected to non-linear soil springs.

5 ACKNOWLEDGEMENT

This work was partly supported by a FRIA FRS-FNRS scholarship. The first author has received funding from the European Unions Horizon 2020 research and innovation programme under the Marie Sklodowska-Curie grant agreement No 753156.

REFERENCES

Achmus, M., C. T. Akdag, & K. Thieken (2013). Load-bearing behavior of suction bucket foundations in sand. *Applied Ocean Research 43*, 157–165.

Achmus, M. & K. Thieken (2010). On the behavior of piles in non-cohesive soil under combined horizontal and vertical loading. *Acta Geotechnica 5*(3), 199–210.

Barnichon, J. (1998). *Finite element modelling in structural and petroleum geology*. Ph. D. thesis, University of Liege, Belgium.

Belgacem, F., P. Hild, & P. Laborde (1998). The mortar finite element method for contact problems. *Mathematical and Computer Modelling 28*(4-8), 263–271.

Bienen, B., J. Dührkop, J. Grabe, M. Randolph, & D. White (2012). Response of Piles with Wings to Monotonic and Cyclic Lateral Loading in Sand. *Journal of Geotechnical and Geoenvironmental Engineering 138*(3), 364–375.

Cerfontaine, B., F. Collin, & R. Charlier (2015). Numerical modelling of transient cyclic vertical loading of suction caissons in sand. *Géotechnique 65*(12).

Cerfontaine, B., A. Dieudonné, J. Radu, F. Collin, & R. Charlier (2015). 3D zero-thickness coupled interface finite element: Formulation and application. *Computers and Geotechnics 69*, 124–140.

Charlier, R. & S. Cescotto (1988). Modélisation du phénomène de contact unilatéral avec frottement dans un contexte de grandes déformations. *Journal de Mécanique Théorique et Appliquée 7*(Suppl. 1).

Goodman, R., R. Taylor, & T. Brekke (1968). A model for the mechanics of jointed rock. *Journal of the Soil Mechanics and Foundations Division 94*.

Guiducci, C., A. Pellegrino, J.-P. Radu, F. Collin, & R. Charlier (2002). Numerical modeling of hydro-mechanical fracture behavior. In *Numerical models in Geomechanics*, pp. 293–299.

Houlsby, G. & B. Byrne (2005). Design procedures for installation of suction caissons in sand. In *Proceedings of ICE, Geotechnical Engineering*, Number July, pp. 135–144.

Houlsby, G., R. Kelly, J. Huxtable, & B. Byrne (2006). Field trials of suction caissons in sand for offshore wind turbine foundations. *Géotechnique 56*(1), 3–10.

Jha, B. & R. Juanes (2014). Coupledmultiphase flow and poromechanics: A computationalmodel of pore pressure effects on fault slip and earthquake triggering. *Water Resources Research 50*, 3776–3808.

Kourkoulis, R., P. Lekkakus, F. Gelagoti, & A. Kaynia (2014). Suction caisson foundations for offshore wind turbines subjected to wave and earthquake loading : effect of soil ? foundation interface. *Géotechnique 64*(3), 171–185.

Olsson, R. & N. Barton (2001). An improved model for hydromechanical coupling during shearing of rock joints. *International Journal of Rock Mechanics and Mining Sciences 38*(3), 317–329.

Reese, L. & W. Van Impe (2010). *Single piles and pile groups under lateral loading* (Second ed.). CRC Press.

Wriggers, P. (2006). *Computational contact mechanics* (Second ed.). Wiley : Chichester.